Seventh International Conference on CFD in the Minerals and Process Industries
CSIRO, Melbourne, Australia
9-11 December 2009

HEMODYNAMIC SIMULATION FOR CONGENITAL HEART DISEASE

J L LIU[1], Y QIAN[1, 4*], M UMEZU[1], K ITATANI[2, 3] and K MIYAJI[2]

[1] Center for Advanced Biomedical Science, TWIns, Waseda University, Tokyo, Japan
[2] School of Medicine, Kitasato University, Kanagawa, Japan
[3] Graduate School of Medicine, The University of Tokyo, Tokyo, Japan
[4] Australian School of Advanced Medicine, Macquarie University, Sydney, Australia
*Corresponding author, E-mail address: sen11@aoni.waseda.jp

ABSTRACT

Hypoplastic left heart syndrome (HLHS) is one kind of congenital heart diseases of newborn. The surgeries for HLHS have to be carried out at very early stage. However, currently there are no quantitative standard to evaluate and predict the outcome of the therapy. In this study, computational fluid dynamics (CFD) is introduced simulate the hemodynamics after Norwood surgery; a first stage surgery for HLHS. Blood flows derived from Echocardiography measurements were used as boundary conditions for pulsatile calculation. The circulations of blood flows were observed and the flow distribution in each vessel is estimated. Energy losses (EL), local pressure, and wall shear stress (WSS) in anastomosis were analyzed to estimate the result of HLHS treatment. The results indicate that pulsatile simulation is essential to quantitatively evaluate the quality of HLHS operation, and the method of computational hemodynamics analysis could be applied into the process of the operations for surgical optimization.

Keywords Hypoplastic left heart syndrome, Norwood operation, computational fluid dynamics, hemodynamics

NOMENCLATURE

α	Womersley Number
ε	turbulent dissipation rate
μ	dynamic viscosity
ρ	density
ω	angular frequency
ΔI	dimension of grid cell
Δt	maximum time step size
f_i	body forces
i, j	coordinate axes
k	turbulent kinetic energy
p	pressure
t	time
$\bar{u}$	time averaged velocity
$\overline{u'}$	fluctuating velocity
C_r	Courant Number
D	characteristic length
E	energy
EL	energy loss
Q	volume flow rate
Re	Reynolds Number
U	velocity

INTRODUCTION

Hypoplastic left heart syndrome (HLHS) is one kind of serious congenital heart diseases (CHD). With a small, underdeveloped left ventricle, a heart suffering from HLHS cannot effectively supply enough blood flow to provide for the needs of the body. In order to improve blood circulation, surgery for HLHS has to be carried out at a very early stage. In general, three-stage palliative surgical management for newborns is now widely accepted (Bove et al, 1996, McGuirk et al, 2005); Norwood, Glenn, and Fontan.

Regarding to the Glenn and Fontan operation, there are almost all published studies were focused on them not only in clinic but also CFD simulation, such as Bove (2003), Migliavacca (1996) and Orlando (2006). Sievers et al (1998) illustrated the turbulence at anastomosis of the total cavopulmonary connection (TCPC) area was the reason of causing energy dissipation, flow disturbances and maldistribution of pulmonary blood flow by applying the methodology of CFD. Whitehead et al (2007) studied the effects of exercise on TCPC power loss and varying relative blood flow to each lung on the power loss under exercise conditions. The analysing methods of CFD on minimizing energy loss under resting conditions or exercise conditions through the connection area to achieve an efficient circulation and evaluate the hemodynamics of operations have made great contribution to the better designs of Fontan operation. The Fontan procedure and its subsequent modifications over the past 30 years can be described as a class of surgical procedure (DeGroff, 2008).

Compared with Glenn and Fontan operation, as the first-stage surgery, Norwood operation, although it plays an important role in the total treatment of HLHS and it has gained popularity as a means of palliating many lesions by creating new local blood circulation to and from lungs around some of the defective areas of the heart, there are currently no quantitative standard to evaluate and predict the outcome of this therapy. Due to the difficulty of studying the outcome directly in vivo, image-based computational fluid dynamics (CFD) was introduced to simulate the blood flow of the Norwood operation.

In present study, a computational hemodynamic analysis system (Qian et al, 2008) which was developed to estimate the rupturing process of cerebral aneurysms was introduced. The promoted CFD methodology to analyse blood flow based on patient-specific geometry, with flow boundary pressure and flow conditions measured in-vivo in Kitasato University Hospital by using a catheter with

pressure sensor and echocardiography. A series of in-vitro verification and validation were carried out, including grid independent and calculation domain influence. The aim of the study was not only to confirm the applicability of the computational hemodynamic analysis system in the HLHS surgical optimization but to disclose the characteristics of local hemodynamics at the area of anastomosis on predicting the outcomes after Norwood operation in clinic by applying the methodology of CFD.

METHODS

The objective of this study is to investigate the relationships between characteristics of local hemodynamics at the area of anastomosis after the Norwood operation and optimization of the operations for surgical treatment of HLHS by using the computational hemodynamic analysis system developed in our previous studies. The image-based analysis approach employed by the system involves the following four steps. First, the patient-specific clinical data after operations are acquired by applying some medical equipment included the geometry of the vessels which will be studied by CT or MRI (Magnetic resonance imaging) scan, the information of physiologically pulsatile blood flow velocity profiles at the inlets by MRI or Echocardiography, and the distribution of blood pressure at the outlets by catheter with pressure sensors. Second, the three-dimension (3-D) geometry of patient-specific vessels are reconstructed by using the geometry function of our analysis system from DICOM files and also converted them into 3-D numerical model at the same time. A number of finite elements are applied to discretize the numerical model area after the conversion for CFD simulation. Third, blood flow simulation with the boundary conditions at the inlets and outlets obtained by the first step are carried out to acquire a set of converged solution for the flow field. Last but not least, several methods of visualization and analysis are applied to analyse the hemodynamic properties of blood flow in patient-specific vessels after operations and to give some suggestions and optimization for the future treatment. The sketch of above process could be shown in Figure 1.

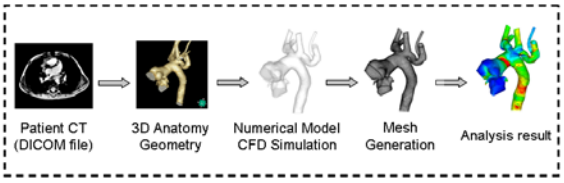

Figure 1: Computational hemodynamic analysis process

Clinical Treatment

A female patient was diagnosed as Hypoplastic Left Heart Syndrome (HLHS), Aortic Stenosis, Hypoplastic Aortic Arch, Coarctation of Aorta, Ventricular Septal Defect (VSD), with echocardiography. She was born after 40-week pregnancy, and was in a shock state due to excessive pulmonary flow on 4 days old. She underwent Norwood procedure (aortic arch repair, Damus-Kay-Stansel anastomosis), right ventricle to pulmonary artery (RV-PA) conduit, and atiral septal defect (ASD) enlargement on 8 days old. With the agreement of the parents and the protocol which had previously received the approval of the local institutional review board and the regional research ethics committee, our patient-specific associated studies were approved.

Numerical Analysis

Blood Flow Governing Equations

The blood flow performed by the computational analysis system of equations is the Navier-Stokes (N-S) equation and continuity equation (1) that describe the most general movement of fluid medium. These equations are defined below.

$$\begin{cases} \dfrac{\partial}{\partial t}(\rho u_i)+\dfrac{\partial}{\partial x_j}(\rho u_i u_j)=-\dfrac{\partial p}{\partial x_i}+\dfrac{\partial}{\partial x_j}\left[\mu\left(\dfrac{\partial u_i}{\partial x_j}+\dfrac{\partial u_j}{\partial x_i}\right)\right]+f_i \\ \dfrac{\partial \rho}{\partial t}+\dfrac{\partial}{\partial x_j}(\rho u_j)=0 \end{cases} \quad (1)$$

where i, j=1,2,3, x_1, x_2, x_3 means coordinate axes, u_i, u_j and p are the velocity vector and the pressure in the point of the fluid domain, ρ and μ are blood density and viscosity, t is time. The term f_i expresses the action of body forces.

Due to the relatively large size of the vessels compared to individual blood cells (McDonald, 1974) and shear rates in lager arteries are typically sufficiently large (Fung, 1981), the blood flows were assumed to be a Newtonian fluid, with constant density (ρ = 1060 kg/m^3) and viscosity (μ =4.0×10^{-3} Pa s) (Linderkamp et al, 1982, Long et al, 2005, Mackintosh, 1973), and the body forces of blood was omitted.

The Reynolds Number (Re) which is expressed the motion of fluid and Womersley Number (α) which is standed for blood flow pulsatile frequency were evaluated respectively by:

$$\mathrm{Re}=\frac{\rho U D}{\mu} \qquad \alpha=\frac{D}{2}\sqrt{\frac{\rho\omega}{\mu}} \quad (2)$$

where the angular frequency (ω) based on the time scale of interest is defined as $\omega = 2\pi/t$. The typical Reynolds number is approximately 4000 in the aorta (Ku, 1997). Therefore, turbulence calculation would be used in the study. For analysis of turbulent flow, instead of N-S equations (1), Reynolds equations (3) were used:

$$\frac{\partial}{\partial t}(\rho\overline{u_i})+\frac{\partial}{\partial x_j}(\rho\overline{u_i}\,\overline{u_j})+\frac{\partial}{\partial x_j}(\rho\overline{u_i'u_j'})=-\frac{\partial p}{\partial x_i}+\frac{\partial}{\partial x_j}\left[\mu\left(\frac{\partial \overline{u_i}}{\partial x_j}+\frac{\partial \overline{u_j}}{\partial x_i}\right)\right] \quad (3)$$

where $\overline{u_1}$, $\overline{u_2}$, $\overline{u_3}$ are time averaged velocity components; $\overline{u_1'}$, $\overline{u_2'}$, $\overline{u_3'}$ are fluctuating velocity components. Different turbulence models are used for a series of these equations.

Because of the relative high-Reynolds number calculated above, the standard k-ε model, developed by Launder and Sharma (Launder and Sharma, 1974), was used in the current study. The standard k-ε model has been very successful in a large variety of different flow situations. In this model, Boussinesq's assumption (4) was employed. The terms $\left(\rho\overline{u_i'u_j'}\right)$ in equations (3) are defined by following expression:

$$\rho\overline{u_i'u_j'}=-\mu_t\left(\frac{\partial \overline{u_i}}{\partial x_j}+\frac{\partial \overline{u_j}}{\partial x_i}\right)+\frac{2}{3}\rho k\delta_{ij} \quad (4)$$

The motion of turbulent fluid could be described by new forms of equations (5) with other two differential equations of turbulent kinetic energy k (6) and turbulent dissipation rate ε (7) which are defined below.

$$\frac{\partial}{\partial t}\left(\rho\overline{u_i}\right)+\frac{\partial}{\partial x_j}\left(\rho\overline{u_i u_j}\right)=-\frac{\partial p}{\partial x_i}+\frac{\partial}{\partial x_j}\left[\left(\mu+\mu_t\right)\left(\frac{\partial\overline{u_i}}{\partial x_j}+\frac{\partial\overline{u_j}}{\partial x_i}\right)-\frac{2}{3}\rho k\delta_{ij}\right] \tag{5}$$

$$\frac{\partial}{\partial t}\left(\rho k\right)+\frac{\partial}{\partial x_j}\left(\rho\overline{u_j}k\right)=\frac{\partial}{\partial x_j}\left(\Gamma_k\frac{\partial k}{\partial x_j}\right)+P_k-\rho\varepsilon \tag{6}$$

$$\frac{\partial}{\partial t}\left(\rho\varepsilon\right)+\frac{\partial}{\partial x_j}\left(\rho\overline{u_j}\varepsilon\right)=\frac{\partial}{\partial x_j}\left(\Gamma_\varepsilon\frac{\partial\varepsilon}{\partial x_j}\right)+\frac{\varepsilon}{k}\left(C_{\varepsilon1}P_k-\rho C_{\varepsilon2}\varepsilon\right) \tag{7}$$

where the term P_k expresses generation of energy k,

$$P_k=-\rho\overline{u_i'u_j'}\frac{\partial\overline{u_i}}{\partial u_j}\qquad \Gamma_k=\mu+\frac{\mu_t}{\sigma_k}\qquad \Gamma_\varepsilon=\mu+\frac{\mu_t}{\sigma_\varepsilon} \tag{8}$$

Parameters ε and μ_t are defined as follows:

$$\varepsilon=\frac{\mu}{\rho}\overline{\left(\frac{\partial u_i'}{\partial x_j}\right)^2}\qquad\qquad \mu_t=\rho C_\mu\frac{k^2}{\varepsilon} \tag{9}$$

the constants of *k*-ε model are as follows: C_μ =0.09, $C_{\varepsilon1}$ =1.44, $C_{\varepsilon2}$ =1.92, σ_k =1.0, σ_ε =1.3. (Launder and Spalding, 1974)

The energy loss (EL) equation (10) was used to verify the grids independence in the CFD simulation and also to evaluate the Norwood operation, which is expressed as below:

$$EL=\sum_{inlet}\left(P_{inlet}+\frac{1}{2}\rho u_{inlet}^2\right)Q_{inlet}-\sum_{outlet}\left(P_{outlet}+\frac{1}{2}\rho u_{outlet}^2\right)Q_{outlet} \tag{10}$$

Geometry Reconsitruction

The cross-sectional images in clinic were acquired by 16-slice multi-detector row enhanced computerized tomography (CT) (BrightSpeed Elite, GE Medical System, Tokyo, Japan). Each slice thickness was 0.625 mm. The series of original cross-sectional CT images was reconstructed by commercial software, RealINTAGE®. A non-shrinking smoothing technique was employed to generate the numerical model for CFD simulation. The accuracy of the reconstructed model had been checked against the true geometry with an exacted measurement. The geometry after smoothing extracted from patient CT images was shown in Figure 2(a).

Mesh Generation

The commercial software, ANSYS®-ICEM 11.0, was applied to the grid generation. In order to accurately measure WSS at near-wall-region, the boundary-fitted prism layers were generated at the boundaries to improve the resolution of the relevant scales in fluid motion. The meshes were shown in Figure 2(a). In present study, there were five layers generated with an average nodal space, increasing by a ratio of 1.3. The distance of the first layer to the vessel surface was fixed at 0.02 mm. The total thickness of the layers was changed with the different branches from 1.3% to 14.5% depending on the average local-vessel diameters.

Because the accuracy of CFD results relies heavily on the grid resolution and boundary conditions, grid quality tests and boundary domain extension tests were carried out using ANSYS® Fluent 6.3.26. As shown in Figure 2(b), when the grid number was around 1,000,000 , the energy loss at the condition of systolic peak, created at calculated domain, started to converge into a constant.

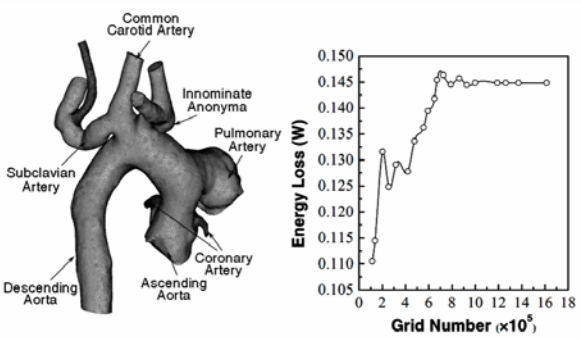

(a) (b)

Figure 2:(a)Geometry with grids (b)Grid independent test

Boundary Conditions

The boundary conditions, at ascending aorta(AAo), pulmonary artery(PA), coronary artery(CA), descending aorta(DA), and neck vessels(NV), including innominate anonyma (IA), common carotid artery (CCA), and left subclavian artery (SA), were respectively measured in-vivo by using an intracardiac catheter with pressure sensor and echoardiography in real-time with ECG (Electro-cardiogram). Detailed information of inlets included AAo and PA was displayed as curves showed in Figure 3.

Furthermore, a relatively long length of the inlet blood vessels extended 20 times of corresponding vessels' diameter allows for fully developing the flow boundary layer at the inlet of the section of AA and PA. The outlet domain for the simulation was extended to be approximately 60-70 times to sufficiently recover the blood pressure at the outlet.

The velocity profile at each inlet of AAo and PA and zero pressure gradients at the outlets of the each extended domain were applied to solve the governing equations in present study. The vessels were presumed as rigid surfaces, including the extension parts.

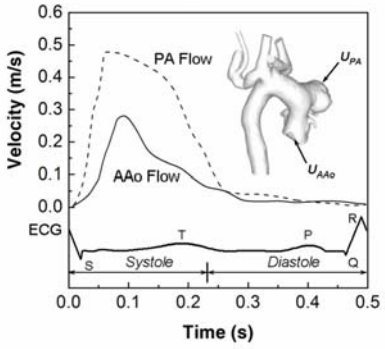

Figure 3: Clinical information as boundary conditions

Calculation

Two numerical solver methods were used in the study separately, a steady state solver and a transient flow

solver. The steady state method solves the non-time dependant form of the N-S equations. For the transient solution method, the Euler method was applied to solve the time-dependent N-S equations.

Moreover, the motion of blood flow in the study is described below. For the steady solution, the time average velocity was 0.41 m/s with a maximum velocity of 0.97 m/s occurring at 0.08s at anastomosis. The characteristic length (D) is 0.0125 m at anastomosis and the average Re was 1358.125 with the corresponding maximum Re was 3213.125. The Womersley Number (α) based on the average cross sectional area was 11.4. Flow in the domain is mainly turbulence. For the transient solution, because of the pulsating flow, the turbulence may occur for a Reynolds Number much large that expected for steady flow. This is due to the fact that an accelerating flow is more stable than steady flow, and also the decelerating flow is more unstable than steady flow (Fung, 1997, Hart, 1997). A critical Reynolds Number (Re_c) for unsteady flow was found by Nerem et al.(1972) This takes the form of Re_c=constant$\times \alpha$, with the constant of proportional ranging from 250 to 1000.(Nerem et al, 1972) In present research, Re_c ranges from 2850 to 11400. The maximum Re in our study is in the critical range.

Therefore, the flow in this study was assumed as unsteady and transition. Because of the relative high-Reynolds number, *k-ε* turbulence model was employed. The simulation was performed for three consecutive cycles at 120 BPM to reach a cyclically repeated solution, and the Courant Number defined below was used to calculate how many time steps would be subdivided in each cycle.

$$C_r = \bar{u}\frac{\Delta t}{\Delta I} \tag{11}$$

where $\bar{u}$ is average velocity, Δt is maximum time step size, and ΔI is the dimension of grid cell. As a general rule the solution is deemed unstable if the Courant Number exceeds 1.0. In present study, equal time step size was applied, Δt =0.00001s, and each cycle was sub-divided into 50000 time steps. The Courant Number ranged from 0.0003 to 0.205. As the convergence criteria, the relative variation of the calculated quantities between two successive iterations was smaller than the pre-assigned maximum residence 10^{-5}.

RESULTS

Figure 4 displays the results of velocity patterns and streamlines at the systolic phase and diastolic phase. Close examination of the instantaneous velocity pattern, at the systolic phase, it shows that high velocity was observed near the outside wall of the AA-PA connection and then turned into the inside of the aortic arch when the blood flow passed the steeply curved aortic arch. At the diastolic phase, the phenomenon still exists.

The results are accordant with the potential flow theory, which predicts a skewing of the velocity profile toward the inner wall of the bend, such as the ascending arch. It is indicated that flow highly changed direction at near the aortic arch. The energy loss and oscillation of the WSS may be caused, which could give a significant influence on the endothelial layer permeability directly.

Contour plots of the total pressure and WSS distribution at six temporal instances, including the systolic phase and diastolic phase, are illustrated in Figure 5. It is obvious that total pressure of the blood fluid is high near the middle position of the aortic arch, whereas a prominent low-pressure area is formed at anastomosis.

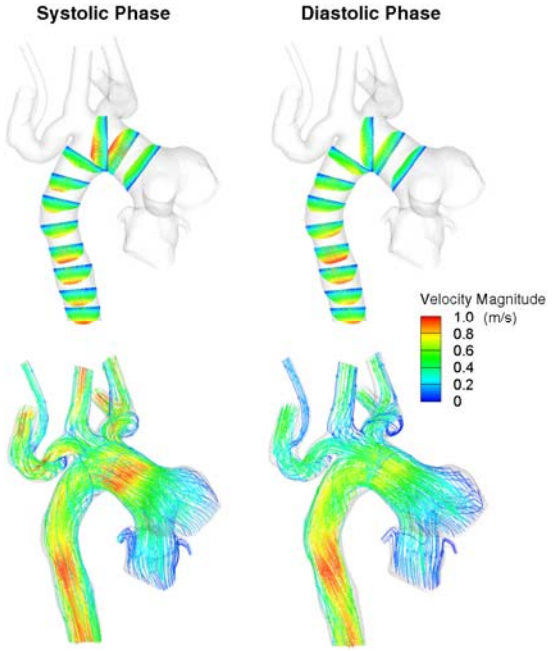

Figure 4: Streamlines of systole and diastole

On the contrary, the distribution of WSS displayed opposite characteristics. Relative high WSS was occurred at the AA-PA connection during the whole cycle. Furthermore, the size and location of the low-pressure area and high WSS area are both variable in one cardiac cycle shown in Figure 5. In addition, the pressure results calculated at the site of AAo, DA, CA and NV were displayed in Figure 6 (a), (b), (c) and (d), respectively.

Both the time-varying energy loss and the average energy loss in one heart cycle were displayed in Figure 7. The maximum energy loss was approximately 0.112W which was generated at the systolic peak, and the average value of the energy loss from pulsatile calculation was 0.0381W. The result was about 1.5 times of the energy loss which calculated by steady calculation.

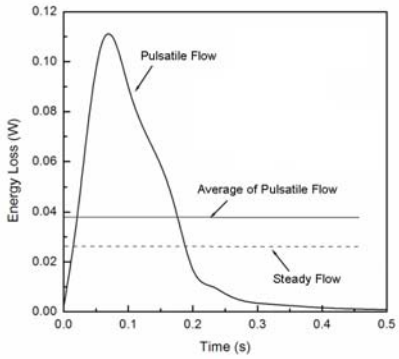

Figure 7: The energy loss in one heart cycle

Furthermore, in one heart cycle the percentage of blood flow distribution at each branch vessels was shown in Table 1.

Percentage of Blood Flow Distribution (%)					
Calculation	DA	IA	CCA	SA	CA
Steady	62.76	14.24	10.51	8.54	3.95
Pulsatile	64.31	13.41	9.53	8.09	4.66

Table 1: Percentage of blood flow distribution

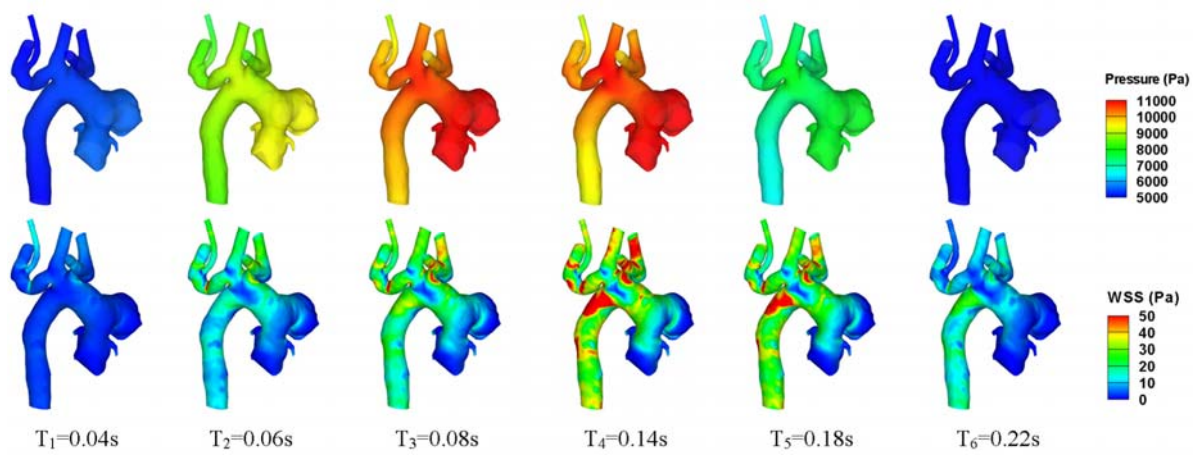

Figure 5: Distribution of instantaneous pressure and wall shear stress (WSS) T_3=0.08s the blood flow arrived at the systolic peak

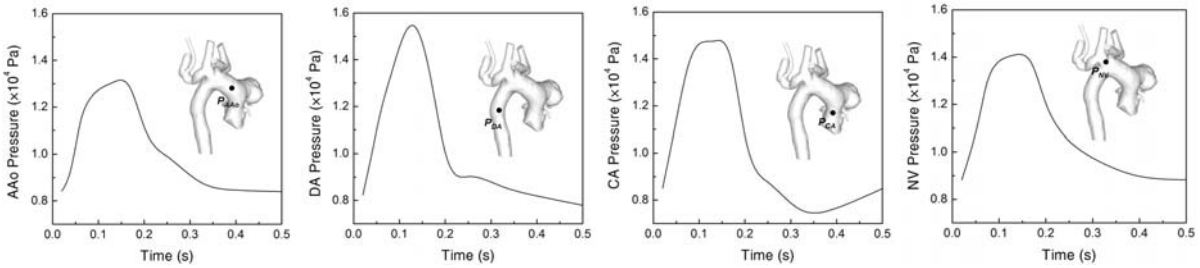

Figure 6: Pressure distribution at AAo (a), DA (b), CA (c) and NV (d)

DISCUSSION

In present study, the CFD system which was verified and validated in-vivo and in-vitro in our previous studies was developed for the systemic quantification and evaluation of the Norwood operation, which was calculated based on the patient-specific reconstructed vessels geometry with physiologically realistic pulsatile flow conditions in vivo. The object of this study is to show the capability and the importance of computational hemodynamic analysis on understanding the local characteristics of hemodynamics in the step-by-step treatment of HLHS for future surgeries. Meanwhile, a well-established analysis approach of CFD based on the clinical images was introduced, which was shown in Figure 1.

In the simulation, computational hemodynamics analysis was used to obtain the blood flow information in details, including WSS, pressure distribution, energy loss, and so on. Furthermore, due to the strong dependence of flow characteristics on the vessel geometry, physiological flow features observed by the hemodynamic reproduced in vitro may display more clearly than that in simplified or idealized arterial models, especially for the surgical optimization. Therefore, the accuracy of the 3-D geometry reconstruction on patient-specific vessels is the key factor in the total numerical analysis. The geometry based on the CT images used in the study is accurate enough satisfying the need of analysis.

The pulsaital flow and steady flow simulation are both been studied in present research. With the comparison of energy loss in the pulsatile simulation and steady simulation in Figure 7, it shows that the average energy loss of pulsatile calculation is as much as two times of steady calculation and the pulsatile flow simulated is more important and necessary than steady flow for analysing local blood energy loss on the quantitative evaluation and prediction of surgical outcomes in details. However, in the practice of clinic, the steady flow information of blood is much easier to be obtained by some techniques, such as MRI, and also bring little pain to the patients than using the Catheter pressure measurement to get the information of realistic pulsatile blood flow. Therefore, to find the relationship of the energy loss between the pulsatile flow and steady flow in prediction surgical outcomes has greatly significant meanings in clinic. The information regarding spatial and temporal patterns of blood flow, including velocity patterns, total pressure and WSS, were contained in the computational results. For the purposes of analysis, total pressure distribution and WSS at some selected time point in one cardiac cycle were displayed. The results of low-pressure area with high WSS on the surface of anastomosis indicated that the energy loss which may be created at these area. Wall shear stress, the

frictional load from the blood vessel wall, is believed to influence the function of the endothelial cells.

Moreover, although vessel's elasticity is an important issue in hemodynamic analysis, especially at the aortas, and the pressure waves calculated perhaps appear a little of delay varying in different parts of the arterial system, the rigid vessel walls were assumed in the simulation and the wall compliance was not considered because of not only a small space in the thorax for children's heart movement but also the postoperative dense adhesion around the reconstructed aortic arch. In addition, from the technique point of view, the simulation of rigid vessels can be finished in a relative short time compared with the simulation of compliance vessels. This makes it possible to apply our methodology directly in the clinical application. The simulation of compliance vessels by using Fluid Structure Interaction (FSI) method takes a huge CPU time. Furthermore, currently, there are no any proper available methodologies which have been validated. Therefore, it is reasonable to simplify the blood vessels as rigid surface in the calculation.

In present study, the purpose of our research is to show the capability and the importance of computational hemodynamic analysis on understanding the local characteristics of hemodynamics at the area of anastomosis after the Norwood operation and optimization of the operations for surgical treatment of HLHS. Hence, the factors of elasticity affect the characteristics of blood flow and pressure did not consider and assumed these arteries as thin-rigid vessels without any movement during the cardiac cycle in present study. In the future, the further study relative to the effects of vessels' elasticity on hemodynamics of blood flow and pressure waves will be carried on.

The important implication contained in the results of this study was very essential for future correlative studies in the outcomes prediction and optimization of HLHS surgeries. Although the patient-specific geometry of vessels before or after operation are different from person to person, the methodology used by our computational hemodynamic analysis system is feasible that would allow the application of CFD analysis into clinical treatment and the process of surgical optimization to establish the quantitative standard in the further studies.

CONCLUSION

Based on the analysis of current study, we can come to the conclusion that the system to be able to quantitatively estimate the quality of CHD surgery has been developed. In-vitro verification and validation processes for grid and boundary condition independent have been carried out. Due to the grid numbers being reduced to an efficient size, the simulation process is able to be performed using a personal computer.

In a future study, the work will centre on further validation not only by the experiment studies which are presently underway in our laboratory but also the methodology employed in our hemodynamic analysis system. A series of before and after cases regarding Norwood surgery will be analysed, as well as systems to be developed for further stage treatments; Glenn and Fontan treatments.

ACKNOWLEDGMENTS

We thank Japanese Ministry of Education, Culture, Sports, Science and Technology (MEXT) for supporting this research. Grant number: A09314800

REFERENCES

BOVE EL, DE LEVAL MR, MIGLIAVACCA F, GUADAGNI G, DUBINI G, (2003), "Computational fluid dynamics in the evaluation of hemodynamic performance of cavo-pulmonary connection after the Norwood procedure for hypoplastic left heart syndrome", *J Thorac Cardiovasc Surg* ,126:1040-1047

BOVE E. L., AND LLOYD T.R., (1996), "Staged reconstruction for hypoplastic left heart syndrome: Contemporary results", *Annals of Surgery* 224(3): 387-395.

KU D.N, (1997), "Blood flow on arteries", *Annual Review of Fluid Mechanics,* 29: 399-434

DEGROFF C.G, (2008), "Modeling the Fontan Circulation: Where We Are and Where We Need to Go", *Pediatr Cardial*, 29: 3-12

FUNG Y. C., (1981) "Biomechanics", *Springer-Verlag*

FUNG Y. C., (1997), "Biomechnics Circulation", *Springer*, New York, Second Edit, Chap 3.

HART, J.D., (1997), "Nonparametric Smoothing and Lack-of-Fit Tests", *Springer-Verlag*, New York, Inc, first edition

LAUNDER. B.E. AND SHARMA. B.I. (1974), "Application of the energy dissipation model of turbulence to the calculation of flow near a spinning disc". *Letters in Heat Mass Transfer*, 1: 131-138

LINDERKAMP O, PAUL Y. K. WU, AND HERBERT J. MEISELMAN, (1982), "Defomability of Density Separated Red Blood Cells in Normal Newborn Infants and Adults", *Pediatr. Res.* 16: 964-964

LONG J. A, AKIF UNDAR, KEEFE B. MANNING, AND STEVEN DEUTSCH, (2005), "Viscoelasticity of Pediatric Blood and its Implications for the Testing of a Pulsatile Pediatric Blood Pump", *American Society of Artificial Internal Organs*, 563-566

MACKINTOSH TF., AND WALKER CHM., (1973), "Blood viscosity in the newborn", *Archives of Disease in Childhood*. 48: 547-553

MCDONALD DA., (1974), "Blood flow in arteries", *Edward Arnold Ltd.*

MCGUIRK S.P., GRISELLI M., STUMPER O.F., RUMBALL E.M., MILLER P, DHILLON R, GIOVANNI J.V., WRIGHT J.G., AND ET AL. (2005), "Staged surgical management of hypoplastic left heart syndrome: a single institution 12-year experience", *Heart* 92: 364-370.

MIGLIAVACCA F, DE LEVAL MR, DUBINI G, PIETRABISSA R (1996) "A computational pulsatile model of the bidirectional cavopulmonary anastomosis: The influence of pulmonary forward flow", *J Biomech Eng* 118: 520-528

NEREM. R. M., SEED. W. A., AND WOOD. N. B., (1972), "An experimental study of the velocity distribution and transition to turbulence in the aorta", *J. Fluid Mech*. 52: 137-160

ORLAMDO W, SHANDAS R, DEGROFF C (2006), “Efficiency differences in computational simulation of the total cavopulmonary circulation with and without compliant vessel walls.” *Compu Meth Prog Biomed* 81: 220-227

QIAN Y, TAKAO H, FUKUI K, UMEZU M, ISHIBASHI T AND MURAYAMA Y, (2008), “Computational Risk Parameter Analysis and Geometric Estimation for Cerebral Aneurysm Growth and Rupture”, *Stroke*: A Journal of the American Heart Association 39: 527-729.

SIEVERS HH, GERDES A, KUNZE J, PFISTER G (1998),“Superior hydrodynamics of a modified cavopulmonary connection for the Norwood operation”, *Ann Thorac Surg* 65:1741-1745

WHITEHEAD KK, PEKKAN K, KITAJIMA H.D, PARIDON S.M, YOGANATHAN A.P AND FOGEL M.A (2007), “Nonlinear Power Loss During Exercise in Single-Ventricle Patients After the Fontan: Insight From Computational Fluid Dynamics”, *Circulation*, 116: 165-171

